Numerical simulation of flow around two side-by-side elliptic cylinders at different Reynolds numbers

Ziming Guo
Harbin Institute of Technology (Weihai), Weihai, China

3162692202@qq.com

Abstract. The study of the flow around the parallel elliptic cylinder is important to the analysis of the shedding vortex, lift, and drag characteristics in practical engineering, while relevant research is limited. In this paper, the flow around two side-by-side elliptic cylinders at different Reynolds numbers (*Re*=100,3900,10^5) is numerically simulated, and the flow characteristics at different gap-ratios and aspect-ratios are analyzed. By comparing the shedding characteristics of the vortexes and the lift ($C_{L,AMP}$ and $\bar{C}_L$)and drag ($\bar{C}_D$) characteristics of the structure, we found that the vortex appears as a single elliptic cylinder at different Reynolds numbers and when *G* is small. Then, with the increase of gap-ratio G, vortexes gradually occur at the gap. Furthermore, $\bar{C}_D$, $C_{L,AMP}$and $\bar{C}_L$ show a decreasing trend. With the increase of aspect-ratio *A*, the size of the vortices in the upper and lower branches decreases at different Reynolds numbers, while the vortexes in the middle branch show different characteristics at different Reynolds numbers.$\bar{C}_D$decreases at different Reynolds numbers as *A* increases. At *Re*=100, with the increase of A, $C_{L,AMP}$ decreases, while $\bar{C}_L$ increases. At *Re*=3900 and *Re*=10^5, The curves of $C_{L,AMP}$ and $\bar{C}_L$show fluctuations.

Keywords: side-by-side elliptic cylinders, gap-ratio, aspect-ratio, the shedding vortex, lift coefficient, drag coefficient.

1. Introduction

In engineering, the phenomenon of the flow around the bluff structure is relatively common. Such as water flowing over piers, ships sailing in the ocean, and so on. At present, the study of flow around two side-by-side cylinders has been sufficient, but that of flow around two side-by-side elliptic cylinders is still missing. The study of flow around two side-by-side elliptic cylinders instructs us to solve some practical problems in engineering situations, such as in the construction and design of catamarans. The study of flow around two side-by-side elliptic cylinders is also helpful to analyze the pressure differential drag data of catamaran sailing, to design the ship type with less drag, which is of great significance for energy saving, environmental protection, and improving economic benefits. In addition, a large number of column structures are often used in Marine structures. Under the action of water flow, the disturbance between multiple cylinders will occur. This disturbance may intensify the vibration of the structure and cause fatigue failure of the column structure. The study of flow around two side-by-side elliptic cylinders is beneficial to the study of the disturbance between elliptic cylinders in engineering.

Currently, there is much research on the flow around the bluff structure. K. Kakuda, et al. simulated the flow field of the cylinder and analyzed the data based on Petrov-Galerkin finite scheme, and obtained the conclusion that as the Reynolds number increases, the separation point of the boundary layer moves backward on the surface of the structure and circulation fields of the near-symmetrical at the back of the cylinder decreases [1]. Based on dynamic Smagorinsky large eddy simulation (LES), I. Afgan, et al., carried out the flow field simulation and data research on two-dimensional two side-by-side cylinders under the condition of subcritical Reynolds number(3900), and the influence of the gap ratio of two side-by-side cylinders on the vortex shedding of the flow field. They found that When the gap ratio increases to a certain value, the cylinder changes from a single bluff body to a biased flow behavior with a bistable flow pattern, and the drag value increases [2]. Now there is also some research on elliptical cylinders. Liu Erpeng, et al. studied the numerical simulation of a single two-dimensional elliptic cylinder under different Reynolds numbers, and analyzed the flow characteristics of the elliptic cylinder under different aspect-ratios (b/a). They found in laminar Reynolds number Vortex shedding at low Reynolds number (100) and subcritical Reynolds number (3900), that the distance between the position and the center of the cylinder increases with the decrease of the axial length ratio [3]. However, this is mostly a study of the flow characteristics of a single elliptic cylinder, and does not involve two side-by-side elliptic cylinders. Y. F.Peng, et al. conducted a detailed numerical simulation study on two side-by-side elliptic cylinders through the immersed boundary method. It is found that in the range of Reynolds less than 100, the lift coefficient decreases with the increase of Reynolds number, while under the same low Reynolds number and the same gap ratio, the lift coefficient increases with the decrease of aspect-ratio. Under the same low Reynolds number and the same gap-ratio, the lift coefficient decreases with the increase of the same gap-ratio [4]. But This study in low Reynolds number is not suitable for all practical situations and does not examine changes in drag coefficients.

Here, we applied the finite element method to explore the two-dimensional problems of viscous incompressible flow around two side-by-side elliptic cylinders. The vortex shedding behind the structure in low and subcritical Reynolds numbers, and the change of lift coefficient and the drag coefficient related to gap-ratio and aspect-ratio under low Reynolds number (100), subcritical Reynolds number (3900) and high Reynolds number (1×10^5) were analyzed. This study focuses on the relationship between vortex shedding characteristics and lift and drag characteristics with aspect-ratio and gap-ratio at different Reynolds numbers. It has a guiding significance for exploring the lift and drag properties of ships and structural fatigue analysis in practical engineering.

2. Numerical simulation method and related model

2.1. Mathematical model

This paper mainly studies the flow around the side-by-side elliptic cylinders in different Reynolds numbers(Re=100,3900,1×10^5). For low Reynolds number, i.e., Re=100, the Laminar model is applied. For subcritical and high Reynolds numbers, i.e. Re=3900 and 1×10^5, the standard k-ε model [5] is applied.

In general, Navier-Stokes equations for incompressible Newtonian fluids in two dimensions are described as follows

$$\frac{\delta ui}{\delta xi}=0 \tag{1}$$

$$-\frac{1}{\rho}\frac{\delta P}{\delta xi}+v\nabla^2 u_i=\frac{\delta u_i}{\delta x_i}+u_j\frac{\delta u_i}{\delta x_j} \tag{2}$$

Where u_i is velocity vector component, x_i, x_j denote the coordinates. ρ denotes the density. P is pressure. The ν is the kinematic viscosity coefficient.

The equations of the standard k-ε model are described below

Turbulent kinetic energy dissipation rate equation

$$\varepsilon = \frac{u}{\rho}\left(\frac{\delta u_i^{'}}{\delta x_k}\right)\left(\frac{\delta u_i^{'}}{\delta x_k}\right) \tag{3}$$

Turbulent viscosity equation

$$\mu_t = \rho C_{mu}\frac{k^2}{\varepsilon} \tag{4}$$

The transport equation of standard k-ε model

$$\frac{\delta(\rho k)}{\delta t} + \frac{\delta(\rho k u_i)}{\delta x_i} = \frac{⬚}{\delta x}\left[\left(\mu + \frac{\delta k}{\delta x_j}\right)\right] + G_k + G_b - \rho\varepsilon - Y_M + S_k \tag{5}$$

$$\frac{\delta(\rho\varepsilon)}{\delta t} + \frac{\delta(\rho\varepsilon u_i)}{\delta x_i} = \frac{\delta}{\delta x_j}\left[\left(\mu + \frac{u_t}{\sigma_\varepsilon}\right)\frac{\delta k}{\delta x_j}\right] + C_{1\varepsilon}\frac{\varepsilon}{k}(G_K + C_{mu}G_B) - C_{2\varepsilon}\rho\frac{\varepsilon^2}{k} + S_\varepsilon \tag{6}$$

In the above equation

$$G_k = \mu_t\left(\frac{\delta u_i}{\delta x_j} + \frac{\delta u_j}{\delta x_i}\right)\frac{\delta u_i}{\delta x_j}, G_b = \beta g_i \frac{\mu_t}{Pr_t}\frac{\delta T}{\delta x_I} \tag{7}$$

$$\beta = -\frac{1}{\rho}\frac{\delta\rho}{\delta T}, Y_M = 2\rho\varepsilon M_t^2, M_t = \sqrt{\frac{k}{a^2}} \tag{8}$$

Where $\mu$is the dynamic viscosity. $G_k$is turbulence caused by the average velocity gradient;$G_b$is the turbulent kinetic energy caused by buoyancy. T is the flow field temperature; YM is the effect of compressible turbulent pulsation expansion on the total dissipation rate; $C_{1\varepsilon}$, $C_{2\varepsilon}$ ⬚ and C_{mu} are empirical constants. ($C_{1\varepsilon}$=1.44,$C_{2\varepsilon}$=1.92, C_{mu}=0.09). $\sigma_K$and$\sigma_\varepsilon$are the corresponding Prandtl coefficient of the turbulent kinetic energy and the dissipation rate of turbulent kinetic energy, respectively.(σ_K=1.0,σ_ε=1.3) .Pr_t is the Prandtl coefficient of turbulence(Pr_t =0.85); g_i is the component of gravitational acceleration in the direction I; $\beta$is the coefficient of thermal expansion; M_t is turbulent Mach number; a is the speed of sound.

The relevant parameters involved in this paper include Re, lift coefficient C_L and drag coefficient C_D, whose equations are as follows

$$\mathrm{Re} = \frac{\rho U L}{\mu} \tag{9}$$

$$C_L = \frac{F_D}{0.5\rho U^2 L}, C_D = \frac{F_L}{0.5\rho U^2 L} \tag{10}$$

Where L is the short axis, and$\mu$is dynamic viscosity. C_L is the component of the force. On the structure in the y direction. C_D is the component of the force on the structure in the x direction.

2.2. *Basin parameters and grid division*

Relevant basin parameters are shown in Figure 1 below. The whole basin is divided into the inner domain (Grid2) and outer domain (Grid1), and the inner field contains two side-by-side static elliptic cylinders, to carry out local mesh thinning technology and reduce the calculation amount. among the basin, the related parameters are as follows. the minor axis L=2b=0.01m.

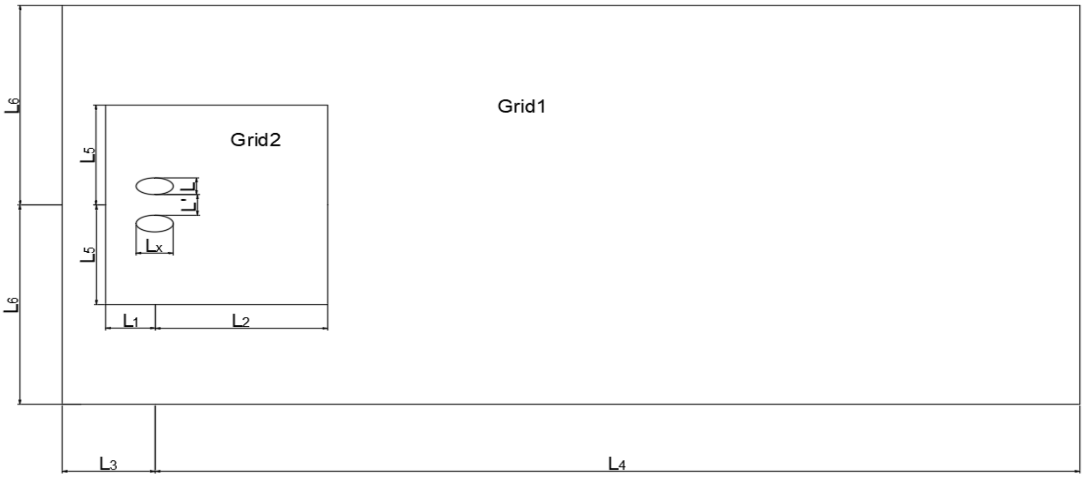

Figure 1. the relevant parameters and the two domains of the basin

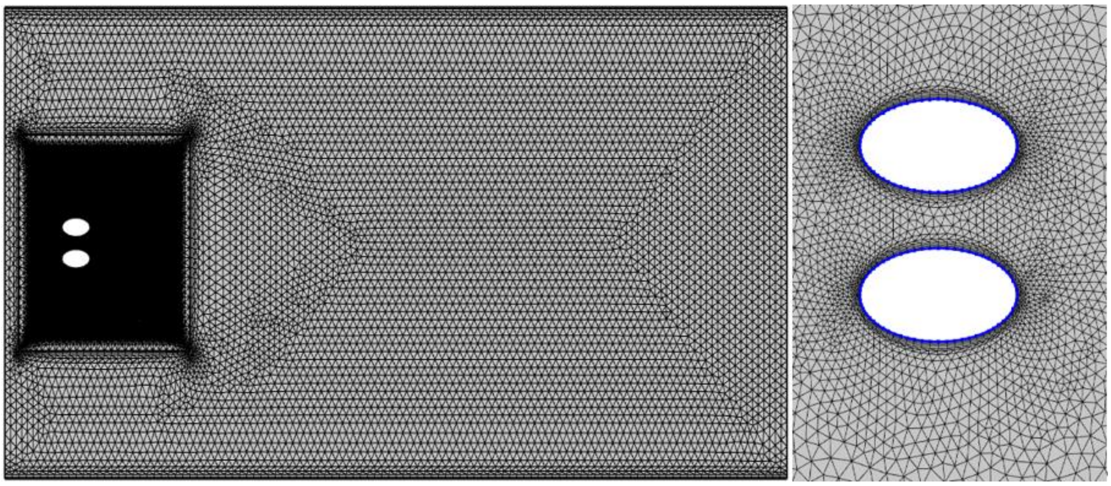

Figure 2. The corresponding mesh division and elliptic cylinders wall local refinement map

The aspect-ratio of the cylinder is A,$i.e.$,$A=\frac{2a}{2b}=\frac{L_x}{L}$. The study is adjusting the value of A by changing the size of a. Various domain lengths used for simulations under the present study are defined as

$$L_1=4L,\ L_2=8L, L_3=5L, L_4=50L, L_5=5.5L, L_6=12L$$

Among the basin, the left boundary is the fluid inlet and the right boundary is the outlet. The upper and lower boundary is set as the external boundary. The fluid inflow velocity u is U and v is 0. And the elliptic cylindrical wall is set to static conditions. Among the outlet domain, the cell size in the grid is $0.5L$. Among the inlet domain, the cell size in the grid is $0.1L$. And the boundary layer mesh is refined for the cylindrical wall as Figure 2 shows. The number of the mesh of the whole domain is 64242.

2.3. The validation of the mesh method

Peng *et al.* have conducted numerical simulation studies at low Reynolds numbers for two attached side-by-side elliptic cylinders [6]. Kim *et al.* studied the numerical simulation for one cylinder when Re=100 [7]. Liu *et al.* have conducted a numerical analysis of subcritical Reynolds numbers and high Reynolds numbers for a single elliptic cylinder [4]. In this study, the simulation results are compared with those of previous studies. As shown in Table 1 below, this model is proven to be effective

Table1. Simulated result of past and corresponding results of this study

Research	Obstacle	Type	*Re*	Parameter	Previous	This study
Peng *et al.*	Attached ellipse	*A*=2	25	$C_{L,Amp}$	0.1148	0.1194
Peng *et al.*	Attached ellipse	*A*=2	30	$C_{L,Amp}$	0.2996	0.2733
Kim *et al.*	Single cylinder	*A*=1	100	$\overline{C_D}$	1.33	1.29
Liu *et al.*	Single cylinder	*A*=1	3900	$\overline{C_D}$	1.09	1.12
Liu *et al.*	Elliptic cylinder	*A*=2	3900	$\overline{C_D}$	0.458	0.412
Zhao *et al.*[8]	Single cylinder	*A*=1	2.5×10^5	$\overline{C_D}$	0.36	0.38

3. Results and discussion

3.1. The characteristics of vorticity in the simulation results

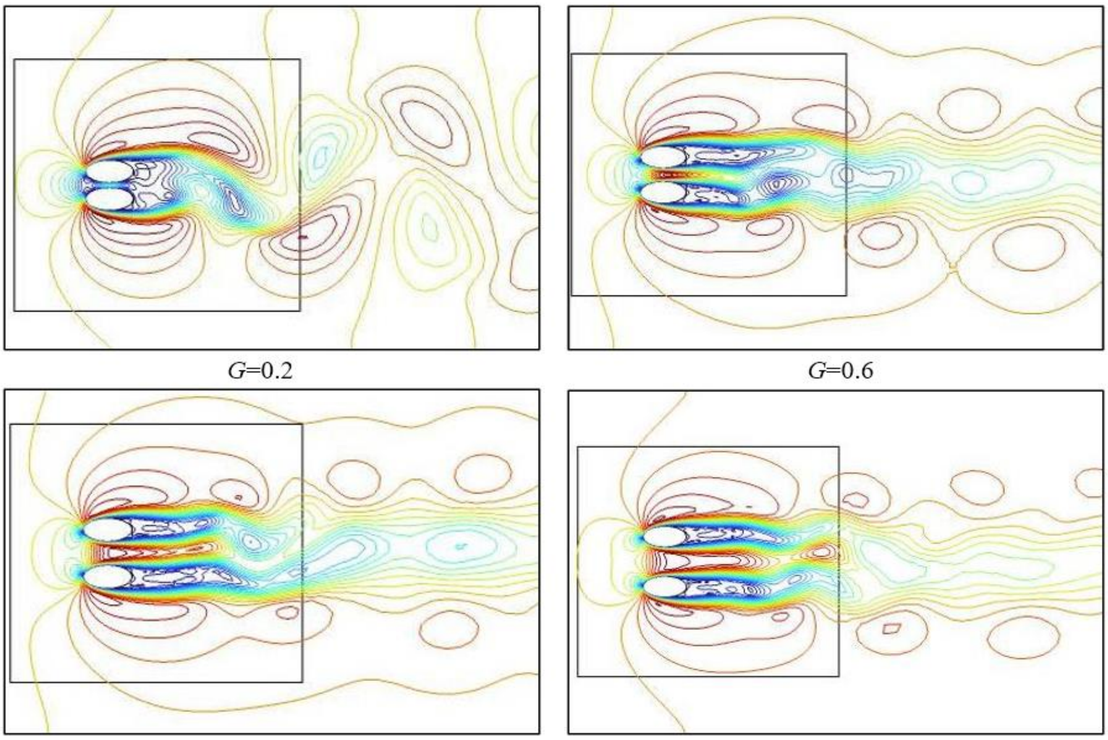

G=0.2 *G*=0.6

G=1 *G*=1.4

Figure 3. Simulated vortexes with various gap-ratio *G*, *A*=2, *Re*=100

First, in the case of *Re*=100, the structures with different aspect ratios *A* and gap-ratios *G* are simulated. As shown in Figure 3, the trailing vortexes in the entire flow field are divided into upper, middle and lower branches. When *G*=0.2, both the upper and lower branches had large vortex shedding, showing periodic shedding. And the middle vortex is smaller. The trailing vortexes of the structure exhibit the properties of flow around a single bigger elliptic cylinder. On the whole, the Karman vortex street phenomenon is obvious. As the *G* increases, the size of the upper and lower vortexes decreases. To the upper and lower branches, the increase in the gap-ratio leads to the influence of the upper and lower separate elliptic cylinders on the vortex, while diminishing the impact of the overall structure. The middle branch of the gap gradually generates and intensifies the vortex. the boundary layer separation of the fluid flowing through the gap takes place, leading to several small vortexes. Then the middle vortexes are formed due to the coupling between the upper and lower small vortexes as Figure 3(*G*=0.6) shows. Then, with the increase of *G*, two separate vortexes gradually appeared behind the two elliptic cylinders respectively, and the coupled vortex alternately fell off at the middle branch, as Figure 3(*G*=1.4) shows. The middle vortex increases, while the upper and lower branch vortex decreases slightly.

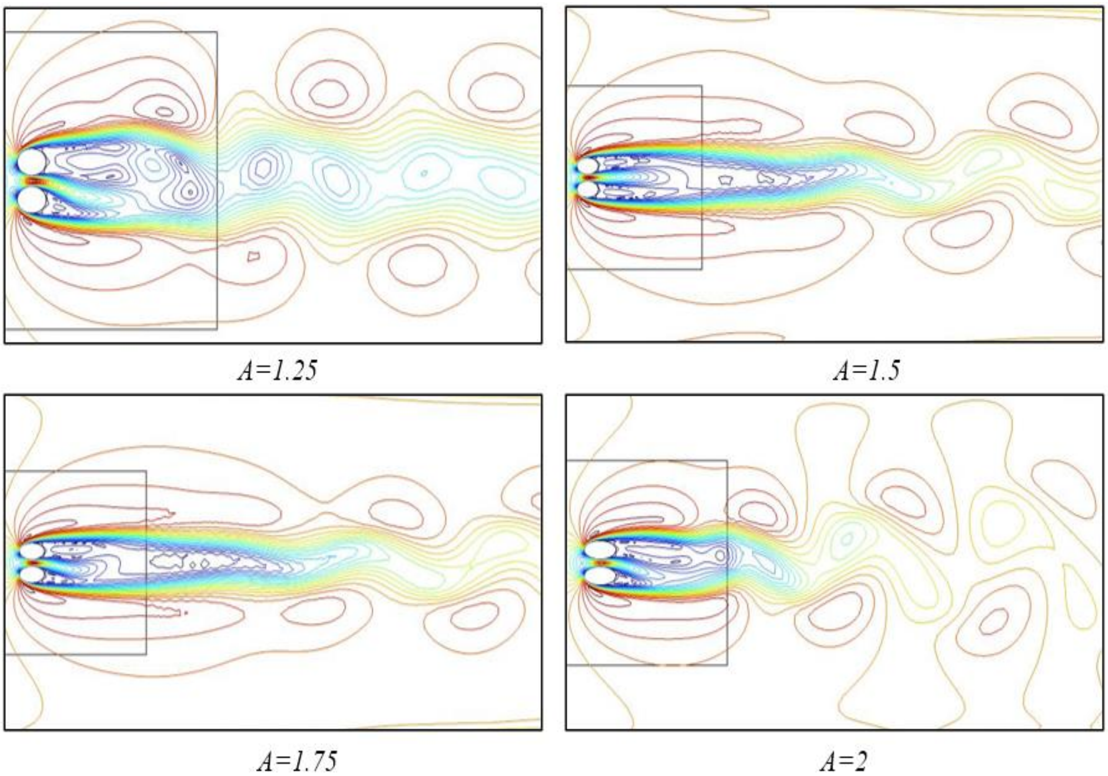

Figure 4. Simulated vortex with various aspect-ratio *A*. *G*=0.4, *Re*=100

Under the condition *Re* = 100, *A* gradually increases. The shedding distance of vortices increases sharply between 1.25 and 1.5, and the middle vortexes slightly decrease, as shown in Figure 4. Then *A* continues to increase, and the growth rate of vortex shedding distance slows down. When the growth of *A* exceeds a certain critical value, the vortex shedding distance begins to decrease. When the *A* increases to 2, the whole structure behaves as a big elliptic cylinder. With the increase of *A*, the shedding distance of the vortex at the upper and lower branches increases at first. And then after *A* reaches some critical value, it starts to decrease. The overall size of the vortex is slightly reduced during the process. When *A* is 2.25, only some small vortexes are generated in the middle branch of the whole flow field.

In the case of *Re*=3900, the structures with different aspect ratios *A* and gap-ratios *G* are simulated. At first, when *G* = 0.4, asymmetrical shedding of small vortexes appears directly behind the two cylinders. In the middle branch, the shedding of vortexes behind a certain elliptic cylinder plays a major role. The vortexes in the upper and lower branches show asymmetrical shedding, and the vortexes are larger. With the increase of *G*, the middle vortex gradually occurs at the gap. The middle vortexes become more and more obvious and dominate in the middle branch. The vortexes at the upper and lower branches also change from the original asymmetric shedding to a more symmetrical shedding. And the shedding distance and size of the vortex decrease with the increase of *G*.

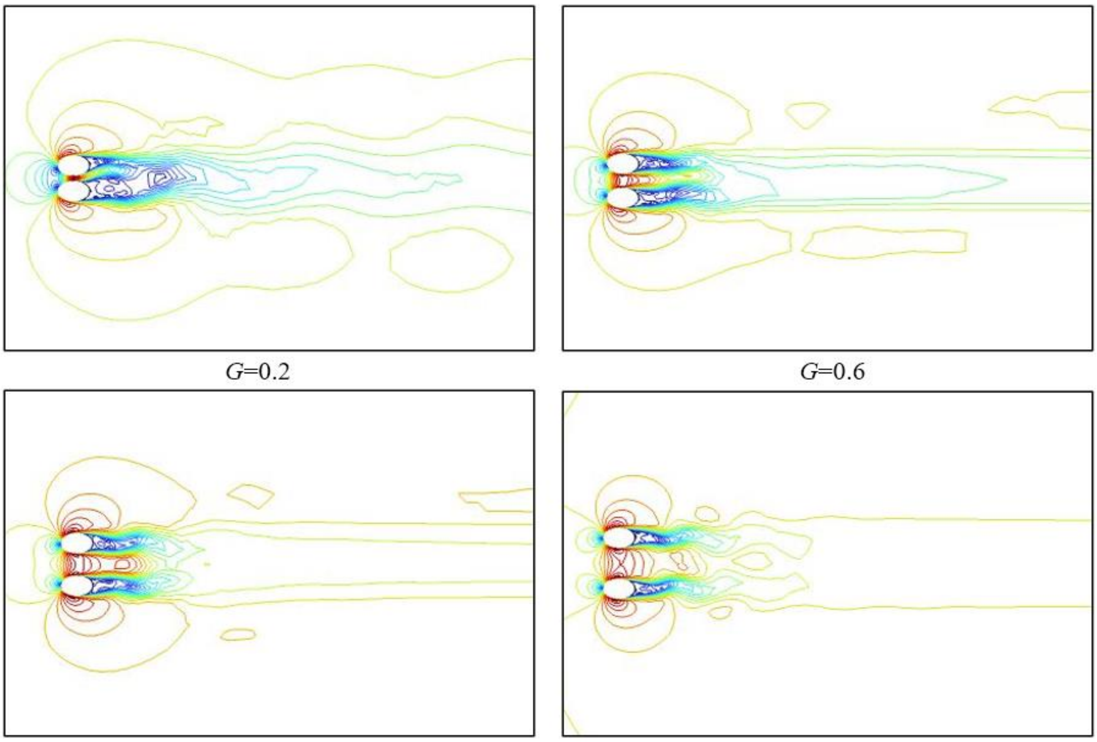

G=0.2 *G*=0.6

G=1 *G*=1.4

Figure 5. Simulated vortex with various gap-ratio *G*. *A*=1.5, *Re*=3900

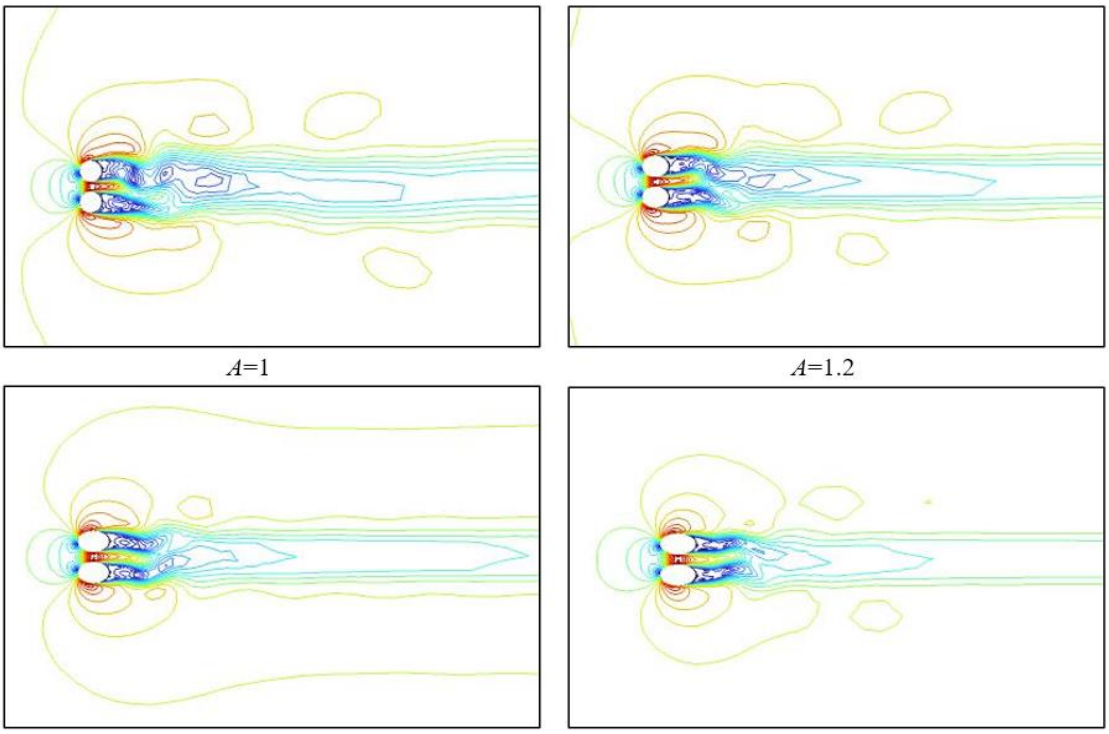

A=1 *A*=1.2

A=1.4 *A*=1.6

Figure 6. Simulated vortex with various aspect-ratio *A*. *G*=0.4, *Re*=3900

As shown in Figure 6, with the increase of *A*, the size of the shedding vortexes at the upper and lower branches gradually decreases, at first, and then increases after *A* reaches a critical value. In general, asymmetric vortex shedding appears at the upper and lower branches. The vortexes shedding occurs behind the two side-by-side elliptic cylinders respectively. Besides, asymmetrically vortexes shedding occurs successively at the middle branches. Moreover, with the increase of *A*, the vortex at the middle branch gradually decreases. This is because the increase of *A* leads to the weakening of boundary layer separation.

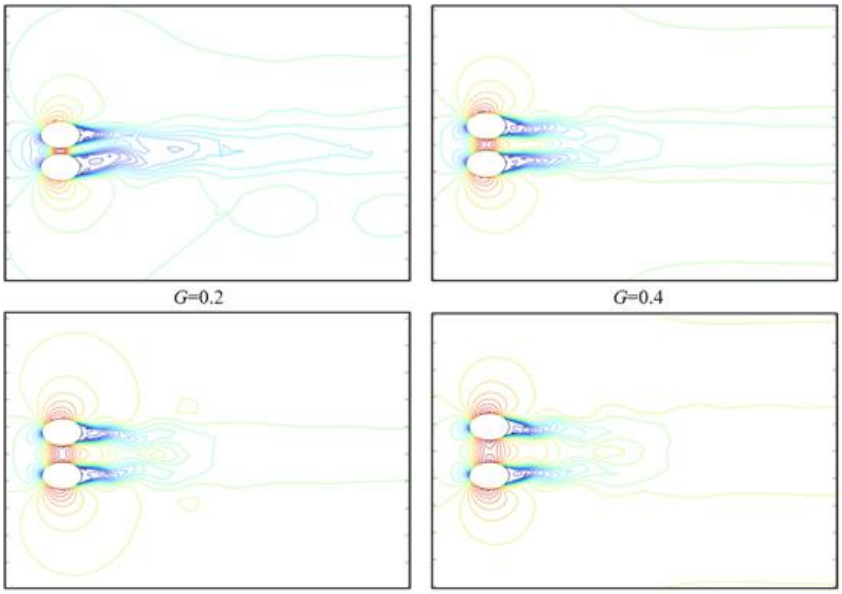

G=0.2 *G*=0.4

G=0.6 *G*=0.8

Figure 7. Simulated vortex with various gap-ratio *G*. *A*=1.5, *Re* $=10^5$

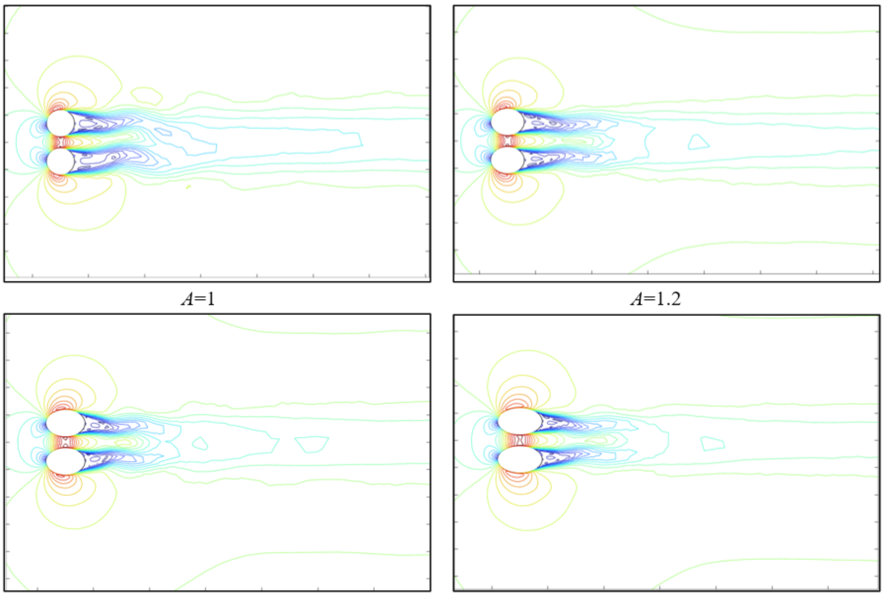

A=1 *A*=1.2

A=1.4 *A*=1.6

Figure 8. Simulated vortex with various aspect-ratio *A*. *G*=0.4, *Re* $=10^5$

Under the condition of the high *Re* $=10^5$, the structures with different *G* and *A* are simulated.

As shown in Figure 7, with the increase of *G*, vortexes generated behind two elliptic cylinders respectively and asymmetrically shedding at the middle branch changes into the gap. Moreover, the size of the vortex generated at the gap gradually increases. Meanwhile, the asymmetric shedding phenomenon of the vortex at the upper and lower branches also changes into a relatively symmetric one.

As shown in Figure 8, when $A = 1$, vortices are generated behind the two side-by-side elliptic cylinders, showing the phenomenon of vortexes asymmetrically shedding at the middle branch, and then with the increase of A, vortexes are generated at the gap and periodically shedding in the middle branch. In the upper and lower branches, the vortexes asymmetrically shed, and the size of the vortex decreases continuously until it is difficult to observe. In general, many small vortexes are generated directly behind the elliptic cylinders.

3.2. *The characteristics of lift and drag coefficient*

The variation of the drag coefficient of the overall structure $\bar{C}_D$ with respect to G is illustrated in Figure 9(a). At Re=3900, the curve exhibits a higher degree of volatility. Overall, there is a decrease in the resistance coefficient as G increases.

The variation of the lift coefficient amplitude of the overall structure $C_{L,AMP}$ with respect to G is illustrated in Figure 9(b). At Re=100, $C_{L,AMP}$ suddenly drops with the G increasing from 0.2 to 0.4. At Re=3900, $C_{L,AMP}$ surges near G =0.4, and then gradually declines. The figures at different Reynolds numbers generally show a downward trend with the increase of G.

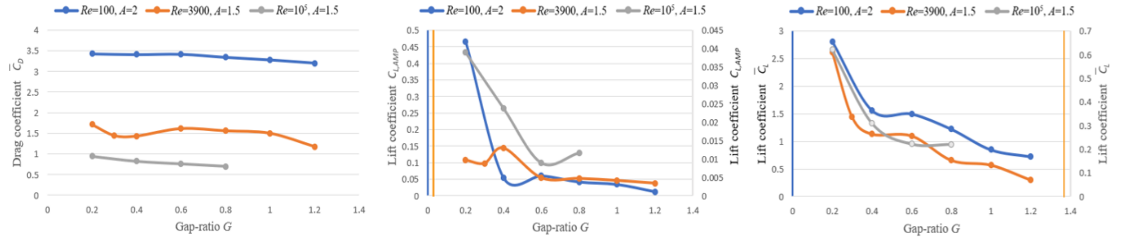

(a)Drag coefficient $\bar{C}_D$ (b) Lift coefficient $C_{L,AMP}$ (c) Lift coefficient $\bar{C}_L$

Figure 9. Change of $\bar{C}_D, C_{L,AMP}$, $\bar{C}_L$ with various gap-ratio G at different Reynolds numbers

The variation of $\bar{C}_L$ with respect to G is illustrated in Figure 9(c). ($\bar{C}_L$ is the maximum of the average lift coefficients of the upper and lower elliptic cylinders) As a whole, $\bar{C}_L$ drops sharply when G increases from 0.2 to 0.4. Then the curve gradually and gently declines.

The variation of $\bar{C}_D$ with respect to A is shown in Figure 10(a). At Re=100, the curve fluctuates at A near 1.4. On the whole, $\bar{C}_D$ tends to decrease with the increase of A under different Reynolds numbers.

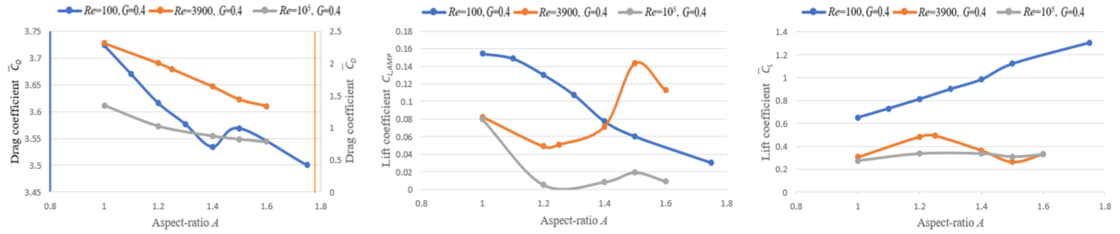

(a)Drag coefficient $\bar{C}_D$ (b) Lift coefficient $C_{L,AMP}$ (c) Lift coefficient $\bar{C}_L$

Figure 10. Change of $\bar{C}_D, C_{L,AMP}$, $\bar{C}_L$ with various aspect-ratio A at different Reynolds numbers

The variation of $C_{L,AMP}$ concerning A is shown in Figure 10(b). At Re=100, the $C_{L,AMP}$ decreases gradually with the increase of A. At Re=3900 and Re=10^5, with the increase of A, $C_{L,AMP}$ first decreases and changes to increase around A=1.2. Then it turns to decrease at around A=1.5.

The variation of $\bar{C}_L$ with respect to A is shown in Figure 10(b). At Re=100, the $\bar{C}_L$ gradually increases with the increase of A. When Re=3900 and Re=10^5, with the increase of A, $\bar{C}_L$ first increases, then changes to decrease around 1.3, and then changes to increase around A=1.5. The transformation of the curve at Re=10^5 is more gentle than that at Re=3900.

4. Conclusion

In this study, the flow around the two side-by-side elliptic cylinders with different gap-ratio G and aspect-ratio is simulated under three conditions, namely, low Reynolds number (Re=100), sub-critical Reynolds number (Re=3900) and high Reynolds number (Re=10^5). The lift and drag characteristics are analyzed. The main conclusions are as follows

(1) Under different Reynolds numbers, when G is small, the whole structure exhibits the flow around a single elliptic cylinder. Then, with the increase of G, vortexes are generated at the middle branch and their size increases gradually. The size of vortices at the upper and lower branches decreases with the increase of G.

(2) At different Reynolds numbers, the size of the vortex at the upper and lower branches decreases with the increase of A. Under Re=100, when A=1.5 and A=1.75, the vortex shedding distance at the middle branch increases sharply. At Re=3900, the vortex asymmetrically sheds at the middle branch. When Re=10^5, with the increase of A, the asymmetric shedding of vortexes at the middle branch changes to generating vortexes at the gap and shedding at the middle branch.

(3) As G increases, $\bar{C}_D$, $C_{L,AMP}$ and $\bar{C}_L$ all show a decreasing trend under different Reynolds numbers. When Re=3900 and A=1.5, $C_{L,AMP}$ change sharply around G=0.4. $\bar{C}_L$ decreases sharply at different Reynolds numbers as G increases from 0.2 to 0.4. On the whole, at Re=3900, the curves of $\bar{C}_D$, $C_{L,AMP}$, $\bar{C}_L$ are relatively volatile.

(4) Under different Reynolds numbers, $\bar{C}_D$ decreases with the increase of A. At Re=100, $C_{L,AMPP}$ decreases with the increase of A. At Re=3900 and Re=10^5, There are inflection points around A=1.2 and around A=1.5 respectively. $\bar{C}_L$ gradually increases with the increase of A at Re=100. When Re=3900 and Re=10^5, there are inflection points around A=1.3 and around A=1.5. The transformation of $\bar{C}_L$ at Re=10^5 is more gentle than that at Re=3900.

References

[1] K. Kakuda, S. Miura, and N. Tosaka, "Finite element simulation of 3D flow around a circular cylinder," *International Journal of Computational Fluid Dynamics,* vol. 20, no. 3-4, pp. 193-209, 2010, doi: 10.1080/10618560600791871.

[2] I. Afgan, Y. Kahil, S. Benhamadouche, and P. Sagaut, "Large eddy simulation of the flow around single and two side-by-side cylinders at subcritical Reynolds numbers," *Physics of Fluids,* Article vol. 23, no. 7, Jul 2011, Art no. 075101, doi: 10.1063/1.3596267.

[3] L. Erpeng, C. Wei, L. Yongshui, W. Siying, and L. Ying, "Numerical simulation of flow around a two-dimensional elliptical cylinder with different Reynolds numbers," *Chinese Journal of applied Mechanics,* vol. 38, no. 05, pp. 2025-2031, 2021. [Online]. Available:.

[4] Y. F. Peng, A. Sau, R. R. Hwang, W. C. Yang, and C.-M. Hsieh, "Criticality of flow transition behind two side-by-side elliptic cylinders," *Physics of Fluids,* Article vol. 24, no. 3, Mar 2012, Art no. 034102, doi: 10.1063/1.3687450.

[5] L. B. E and S. D. B, "Lectures in mathematical models of turbulence," *New York: Academic Press,* 1972.

[6] R. M. Yih-Ferng Peng , A. S. , and R. R. H. , "Nested Cartesian grid method in incompressible viscous fluid flow," 2010.

[7] J. Kim, D. Kim, and H. Choi, "An Immersed-Boundary Finite-Volume Method for Simulations of Flow in Complex Geometries," *Journal of Computational Physics,* vol. 171, no. 1, pp. 132-150, 2001. [Online]. Available:

[8] J. W. Zhiming Zhao, Yigang Gong and Haibo Xu, "Large Eddy Simulation of Flow and Separation Bubbles Around a Circular Cylinder from Sub-critical to Super-critical " *Journal of Marine Science and Application,* vol. 22, no. 02, pp. 219-231, 2023.